

P-type cold-source field-effect transistors with TcX_2 and ReX_2 (X=S, Se) cold source electrodes: A computational study

Qianwen Wang(汪倩文), Jixuan Wu(武继璇), Xuepeng Zhan(詹学鹏), Pengpeng Sang(桑鹏鹏), and Jiezhi Chen(陈杰智)

Citation: Chin. Phys. B, 2023, 32 (**12**): 127203. DOI: 10.1088/1674-1056/ad0116
Journal homepage: http://cpb.iphy.ac.cn; http://iopscience.iop.org/cpb

What follows is a list of articles you may be interested in

MatChat: A large language model and application service platform for materials science

Zi-Yi Chen(陈子逸), Fan-Kai Xie(谢帆恺), Meng Wan(万萌), Yang Yuan(袁扬), Miao Liu(刘淼), Zong-Guo Wang(王宗国), Sheng Meng(孟胜), and Yan-Gang Wang(王彦棡)
Chin. Phys. B, 2023, 32 (**11**): 118104. DOI: 10.1088/1674-1056/ad04cb

Tuning the particle size, physical properties, and photocatalytic activity of Ag_3PO_4 materials by changing the Ag^+/PO_4^{3-} ratio

Hung N M, Oanh L T M, Chung D P, Thang D V, Mai V T, Hang L T, and Minh N V
Chin. Phys. B, 2023, 32 (**3**): 038102. DOI: 10.1088/1674-1056/ac84ce

Robustness of the unidirectional stripe order in the kagome superconductor CsV_3Sb_5

Bin Hu(胡彬), Yuhan Ye(耶郁晗), Zihao Huang(黄子豪), Xianghe Han(韩相和), Zhen Zhao(赵振),Haitao Yang(杨海涛), Hui Chen(陈辉), and Hong-Jun Gao(高鸿钧)
Chin. Phys. B, 2022, 31 (**5**): 058102. DOI: 10.1088/1674-1056/ac5888

Current diffusion and efficiency droop in vertical light emitting diodes

R Q Wan(万荣桥), T Li(李滔), Z Q Liu(刘志强), X Y Yi(伊晓燕), J X Wang(王军喜), J H Li(李军辉), W H Zhu(朱文辉), J M Li(李晋闽), L C Wang(汪炼成)
Chin. Phys. B, 2019, 28 (**1**): 017203. DOI: 10.1088/1674-1056/28/1/017203

Recent observations of negative longitudinal magnetoresistance in semimetal

Xi-Tong Xu(许锡童), Shuang Jia(贾爽)
Chin. Phys. B, 2016, 25 (**11**): 117204. DOI: 10.1088/1674-1056/25/11/117204

SPECIAL TOPIC — Post-Moore era: Materials and device physics

P-type cold-source field-effect transistors with TcX_2 and ReX_2 (X = S, Se) cold source electrodes: A computational study

Qianwen Wang(汪倩文)[1], Jixuan Wu(武继璇)[2], Xuepeng Zhan(詹学鹏)[2], Pengpeng Sang(桑鹏鹏)[2,†], and Jiezhi Chen(陈杰智)[2,‡]

[1] *School of Information Science & Technology, Qingdao University of Science & Technology, Qingdao* 266000, *China*
[2] *School of Information Science and Engineering, Shandong University, Qingdao* 266000, *China*

(Received 26 July 2023; revised manuscript received 12 September 2023; accepted manuscript online 7 October 2023)

Cold-source field-effect transistors (CS-FETs) have been developed to overcome the major challenge of power dissipation in modern integrated circuits. Cold metals suitable for n-type CS-FETs have been proposed as the ideal electrode to filter the high-energy electrons and break the thermal limit on subthreshold swing (SS). In this work, regarding the p-type CS-FETs, we propose TcX_2 and ReX_2 (X = S, Se) as the injection source to realize the sub-thermal switching for holes. First-principles calculations unveils the cold-metal characteristics of monolayer TcX_2 and ReX_2, possessing a sub-gap below the Fermi level and a decreasing DOS with energy. Quantum device simulations demonstrate that TcX_2 and ReX_2 can enable the cold source effects in WSe_2 p-type FETs, achieving steep SS of 29–38 mV/dec and high on/off ratios of (2.3–5.6) $\times 10^7$. Moreover, multilayer ReS_2 retains the cold metal characteristic, thus ensuring similar CS-FET performances to that of the monolayer source. This work underlines the significance of cold metals for the design of p-type CS-FETs.

Keywords: cold metal, steep-slope transistor, subthreshold swing, quantum device simulations

PACS: 72.90.+y, 81.05.Zx, 05.60.Gg, 85.30.Tv **DOI:** 10.1088/1674-1056/ad0116

1. Introduction

With the intensely increasing demands for miniaturization and integration of field-effect transistors (FETs), power dissipation has been one of the major challenges limiting the performance of modern nanoelectronics circuits.[1,2] Power consumption mainly includes dynamic switching dissipation and static leakage consumption.[3] Both dynamic and static power consumption are related to the supply voltage.[4,5] Consequently, reducing the supply voltage, while simultaneously ensuring a low off-state current (I_{off}), is an effective way to relieve the consumption issue. Therefore, it is highly desired for the steep-slope from off-state to on-state. Researchers have made tremendous efforts on the aspects of materials and device principles. On the one hand, numerous two-dimensional (2D) materials have emerged as promising candidates because of their atomically thin thickness and smooth surface, such as transition metal dichalcogenides (TMD),[6,7] group-VA semiconductors,[8,9] and recent emerging MA_2Z_4 family.[10–13] On the other hand, many novel device models have been proposed to achieve steep-slope FETs with the ultra-steep subthreshold swing (SS). SS is the key parameter to evaluate the switching slope of devices and plays a crucial role in power optimization. However, there is a limitation for the SS in conventional MOSFETs, which cannot be lower than 60 mV/dec at room temperature because of the Boltzmann thermal distribution of carriers. Steep-slope devices with sub-60 mV/dec SS have attracted much attention. Tunneling FETs (T-FETs)[14–20] and negative capacitance FETs (NC-FETs)[21–24] have been proposed to break the SS limitation. However, T-FETs and NC-FETs usually suffer from some issues of small drive currents and large hysteresis, respectively. By modulating the density of states (DOS) of the source electrode, the recently proposed cold source FETs (CS-FETs) can realize the steep switching and high on-state current (I_{on}) simultaneously.[25–28] Structures including Dirac semimetals,[25] semiconductors,[29] isolated states,[30,31] and tunneling junctions[32] have been proposed as the source electrodes of CS-FETs. However, these structures have to be artificially doped, which is challenging for two-dimensional semiconductors.

Recently, a type of cold metal material was discovered,[33,34] which is intrinsic metal but possesses a gap in the conduction band (CB) or valence band (VB) around the Fermi level (E_F). It can effectively filter out the carriers' thermal tails (high-energy electrons or holes) and thereby achieve the sub-60 mV/dec SS. Cold metals can directly serve as injection electrodes without artificial doping. Typical cold metals NbX_2 and TaX_2 (X = S, Se, Te) feature an energy gap above E_F due to one fewer electron than semiconducting MoX_2 and WX_2, and are similar to p-type doped semiconductors. Hence, NbX_2 and TaX_2 can filter the high-energy electrons above E_F and are suited for n-type CS-FETs (CS-nFETs).[33] Our prior

†Corresponding author. E-mail: ppsang@sdu.edu.cn
‡Corresponding author. E-mail: chen.jiezhi@sdu.edu.cn

© 2023 Chinese Physical Society and IOP Publishing Ltd

research has revealed that the energy gap below E_F or the decreasing DOS with lower energy is necessary to cut-off or suppress hole tails and realizes p-type CS-FETs (CS-pFETs).[29] Hence, it is important to explore and design the potential cold metals for CS-pFETs.

In this work, regarding the CS-pFETs, we theoretically propose TcX_2 and ReX_2 (X = S, Se) as cold metals aiming at the steeper switching for hole transports. Different from prior NbX_2 (TaX_2), TcX_2 and ReX_2 possess one more electron than that of the typical MoX_2 and WX_2 semiconductors. The desired energy gap for CS-pFETs can be expected in TcX_2 and ReX_2, which can effectively filter out the high-energy holes and achieve sub-60 mV/dec SS. Based on the first-principles calculations, the electronic properties of TcX_2 and ReX_2 are systemically analyzed and their cold-metal characteristics are revealed. Moreover, taking WSe_2 pFET as an example, the steep switching performance is demonstrated by using TcX_2 and ReX_2 as injection sources, systemically verifying the cold-metal effects in device switching. Besides, the thickness influences of cold metals on the switching properties of CS-FETs are also discussed.

2. Methodology

The geometric and electronic properties were computed in the framework of density functional theory (DFT) implemented in the QuantumATK package.[35] The ion–electron interactions were treated by using the PseudoDojo norm-conserving pseudopotential.[36] The exchange–correlation functional was treated by the Perdew Burke Ernzerhof within generalized gradient approximation (GGA).[37] Geometric structures were fully relaxed with a force tolerance of less than 0.01 eV/Å. The Brillouin zone sampling of $12 \times 12 \times 1$ Monkhorst–Pack k-points was employed. The vacuum space was set to be 20 Å to avoid the interactions between material and its periodic images.

The device transport performance was simulated by using DFT coupled with the nonequilibrium Green's function (NEGF) method. The k-points were chosen as $1 \times 1 \times 150$ for device self-consistent calculations. The current was calculated by using the Landauer–Büttiker formula[38]

$$I_d = \frac{2e}{h}\int_{-\infty}^{+\infty}\{T(E)[f_s(E-\mu_s)-f_d(E-\mu_d)]\}\,dE,$$

where $f(E)$ is the Fermi–Dirac distribution function; $\mu_{s/d}$ is the Fermi level of the source/drain electrode; and $T(E)$ is the transmission coefficient from the source to drain. The electrode temperature was set to 300 K.

3. Results and discussion

As shown in Fig. 1, the calculated band structures of TcX_2 and ReX_2 present similar shapes to those of NbX_2 and TaX_2. However, the Fermi level crosses through the CB of TcX_2 and ReX_2, which is different from NbX_2 and TaX_2 with the Fermi level crossing through the VB. This is related to the electron numbers in the outmost shells of transition metal atoms. In comparison to semiconducting MoX_2 and WX_2, TcX_2 and ReX_2 can be seen as naturally n-doped semiconductors. There is an energy gap below the Fermi level, which is referred to as the sub-gap as marked in Fig. 1. It is the sub-gap that breaks up the continuous DOS distributions around E_F and can filter out the holes with energies in the sub-gap. The energy difference between E_F and the conduction band minimum (CBM)

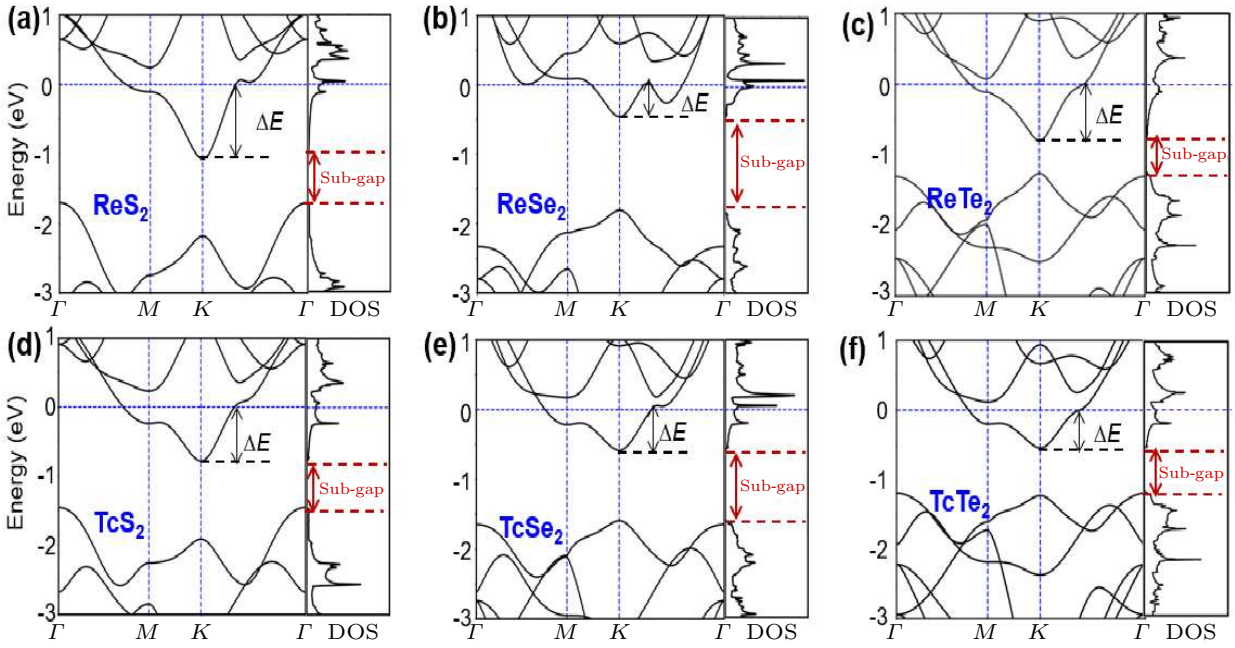


Fig. 1. Band structures and DOSs of monolayer TcX_2 and ReX_2 (X = S, Se, Te). The Fermi level is set to zero.

is denoted by ΔE. It should be pointed out that the ΔE determines the number of carrier thermal tails involved in device transport, whereas the sub-gap determines the number of thermal tails that are cut off. Hence, the larger sub-gap and smaller ΔE are desired for effectively cut off thermal tails. As shown in Fig. 1, the ΔE (sub-gaps) are calculated to be 1.08 (0.63 eV), 0.79 (0.68 eV), 0.46 (1.35 eV), 0.59 (1.01 eV), 0.46 (0.80 eV) and 0.55 (0.65 eV) for ReS_2, TcS_2, $ReSe_2$, $TcSe_2$, $ReTe_2$ and $TcTe_2$, respectively. It is found that the Se- and Te-series possess smaller ΔE than the S-series, besides, the Se-series possesses larger sub-gaps than the S- and Te-series. Hence, the Se-series exhibits more advantages in cutting off the hole tails. Although the ΔE of 0.79–1.08 eV is slightly too large for ReS_2 and TcS_2 to directly cut off thermal tails, the significantly decreasing DOS below the Fermi level can also effectively suppress the spread of hole tails. Given the cold-metal characteristics with a sub-gap or decreasing DOS below the Fermi level, TcX_2 and ReX_2 are expected to serve as the injection source of p-type FETs (pFETs) and realize the cold source effects. Moreover, the calculated band structures in the presence of spin–orbital coupling (SOC) are shown in Fig. S1 of the supporting information. The SOC impacts can be ignored for TcX_2. Although the SOC induces obvious splitting at the k-point of valence bands for ReX_2, the critical sub-gap and ΔE are slightly affected for ReS_2 and $ReSe_2$. Hence, the SOC is predicted to be free of influence on transport properties when TcX_2, ReS_2, and $ReSe_2$ serve as the injection source. Although ΔE is going to vanish, $ReTe_2$ shows cold-metal characteristics with a decreasing DOS.

To verify the role of cold metals (TcX_2 and ReX_2) for p-type CS-FETs, we construct heterojunction FETs with monolayer $ReSe_2$ acting as the injection source, as shown in Fig. 2(a). The lateral heterostructures are experimentally feasible and can be obtained by edge-epitaxial growth in experiments.[39] The intrinsic and p-type doped WSe_2 monolayer serves as the channel and drain electrode, respectively. The intrinsic WSe_2 channel is sandwiched between two 0.41 nm SiO_2 (with a dielectric constant of 3.9) layers, with a gate length (L_g) of 6.6 nm. The drain electrode is doped with a hole concentration of 0.02 per atom to ensure the Fermi level aligns with or down to the valence band maximum (VBM) of WSe_2. Due to the lattice mismatch, two different contact models are considered: (i) the biaxial compressive strain of -1.1% is applied on monolayer $ReSe_2$, while the contacted WSe_2 is free of strain to preserve its intrinsic transport properties for comparison; (ii) the tensile strain of 1.1% is applied on WSe_2 channel, while the ReS_2 metal is free of strain to verify its intrinsic cold-metal characteristic. The ballistic transports of the $ReSe_2$–WSe_2 FET are simulated under the drain-source voltage V_{ds} of -0.5 V. The results are presented in Fig. 2(b) (see the red lines). For comparisons,

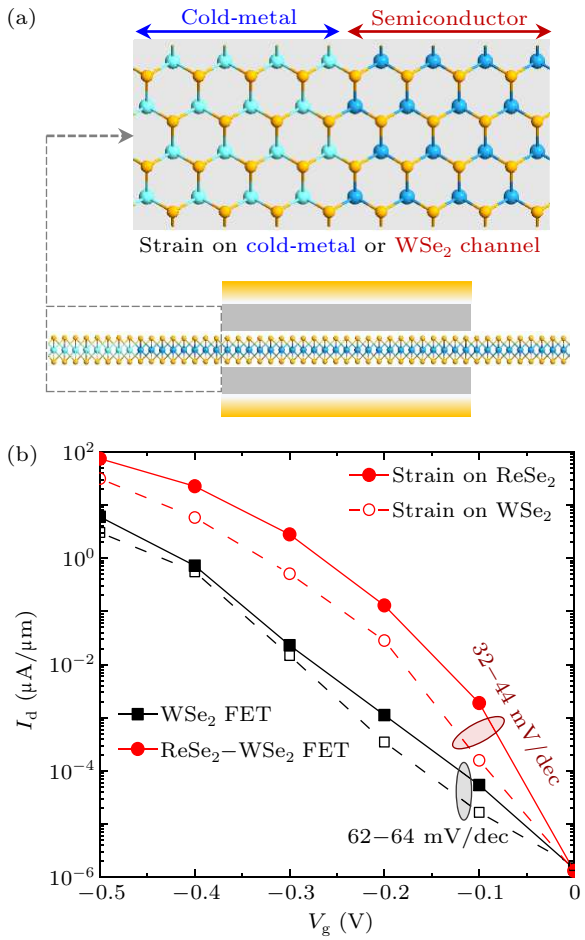


Fig. 2. (a) Schematic device structure of $ReSe_2$–WSe_2 heterojunction CS-FETs with $ReSe_2$ acting as injection source. (b) Comparisons of transfer characteristics between $ReSe_2$–WSe_2 CS-FET (red lines) and WSe_2 MOSFET (black lines); the solid and open points represent the ReS_2 electrode and WSe_2 channel undergoing the mismatch strain, respectively.

the conventional WSe_2 MOSFET is also simulated with the p-doped WSe_2 serving as the injection source, and the results are also listed in Fig. 2(b) (see the black lines). The solid points represent the pristine WSe_2 channel (contacting the strained ReS_2 electrode), while the open points represent the strained WSe_2 channel (contacting the pristine ReS_2 electrode). It is found that the SS as steep as 32–44 mV/dec is achieved for $ReSe_2$–WSe_2 FET with $ReSe_2$ cold source, which breaks the thermal limitation of 60 mV/dec and is much lower than the result of WSe_2 MOSFET with p-doped WSe_2 source (62–64 mV/dec). The sub-60 mV/dec SS is obtained over eight decades of currents from 10^{-6} μA/μm to 10^{2} μA/μm. Moreover, the off-state currents (I_{off}) are defined around 10^{-6} μA/μm and extracted at the gate voltage $V_g = 0$ V, and then the on-state currents (I_{on}) are obtained at $V_{on} = V_{off} - V_{ds}$. By using the constant current definition, the steeper SS results in a larger I_{on} at a finite gate voltage range. However, the larger I_{on} does not mean larger saturation currents. By employing the cold metal $ReSe_2$ as the injection source, the I_{on} of the WSe_2 FET is improved by one order of magnitude from 3–6 μA/μm to 32–75 μA/μm. It is found that

the tensile strain degenerates WSe_2 transport properties and the slight compressive strain can promote the cold-source effects of ReS_2 metal.

To uncover the physical mechanism of cold metal injection, we further present the source DOS and calculate the corresponding hole density $n(h)$ distribution by using the Fermi–Dirac function $f(E)$, $n(h) = f(E) \times \mathrm{DOS}(E)$. The spectrum currents $\mathrm{d}I$ and energy-resolved current density, are also calculated at the on-/off-state. The results are shown in Fig. 3, where the source Fermi level (E_{FS}) was set to 0 eV. Benefitting from the sub-gap below E_{F} in $ReSe_2$, the hole tails with energy lower than 0.35 eV are effectively cut off (see Fig. 3(a)). Consequently, the transmission currents from off-state to on-state are mainly from the holes located around the E_{FS}. The thermal leakage currents are abruptly cut off at the energy range lower than 0.35 eV, which is the origin of the sub-60 mV/dec SS. While for the p-doped WSe_2 source, the continuous DOS below E_{F} results in the continuous hole tails spreading to −0.75 eV and below (see Fig. 3(b)). The spread tails usually lead to hole leakages from the source to the drain and are not conducive to gate modulation. As a result, the transmission currents from off-state to on-state possess a wide range spreading to −0.61 eV and below, which is quite different from the results of cold-metal sources.

We proceed to study the other cold metals when applied to an injection source for WSe_2 pFETs. The $ReTe_2$ and $TcTe_2$ metals are not further considered as the source because of the large lattice mismatch of over 11% with the WSe_2 channel. The device structure shown in Fig. 2(a) is employed with the $ReSe_2$ monolayer replaced by ReS_2, TcS_2, and $TcSe_2$ monolayers, respectively. To avoid the strain influences on the WSe_2 channel and facilitate direct comparison between the results, we mainly discuss the contact model where the lattice mismatch at the interface is entirely applied on cold metals with a biaxial strain of −0.3%, 0.4%, and −3.4% for ReS_2, TcS_2, and $TcSe_2$ monolayers, respectively. It notes that experimental measurements have shown that 2D TMDs can withstand very large deformations of about 10% effective in-plane strain.[40] The simulated I_{d}–V_{g} curves are shown in Fig. 4(a). The studied ReX_2 and TcX_2 (X = S, Se) injection sources all enable steeper slopes than the p-doped WSe_2 source and lift the currents from $\sim 10^{-6}$ μA/μm approaching 10^2 μA/μm within V_{g} of −0.5 V. We further extract the current on/off ratio ($I_{\mathrm{on}}/I_{\mathrm{off}}$) and the SS, as listed in Fig. 4(b). It is found that the sub-thermal switches were all achieved with the SS of 38 mV/dec, 33 mV/dec, 32 mV/dec, and 29 mV/dec for ReS_2, TcS_2, $ReSe_2$, and $TcSe_2$ monolayer source, respectively. Benefitting from the steep slope, the $I_{\mathrm{on}}/I_{\mathrm{off}}$ as large as 2.3×10^7, 2.5×10^7, 5.6×10^7, and 5.1×10^7 are obtained for WSe_2 pFETs with ReS_2, TcS_2, $ReSe_2$, and $TcSe_2$ monolayer source, respectively. The results are five or ten times higher than that of the normal WSe_2 MOSFET (4.1×10^6). Moreover, we also simulate the contact model where the interfacial mismatch is entirely applied on the WSe_2 channel, and the results can be found in Fig. S1 of the supporting information. The strain-free ReX_2 and TcX_2 both can break the thermal limitation and promote the steep SS with values of 33–44 mV/dec. The corresponding $I_{\mathrm{on}}/I_{\mathrm{off}}$ is as high as (2–8)×10^7.

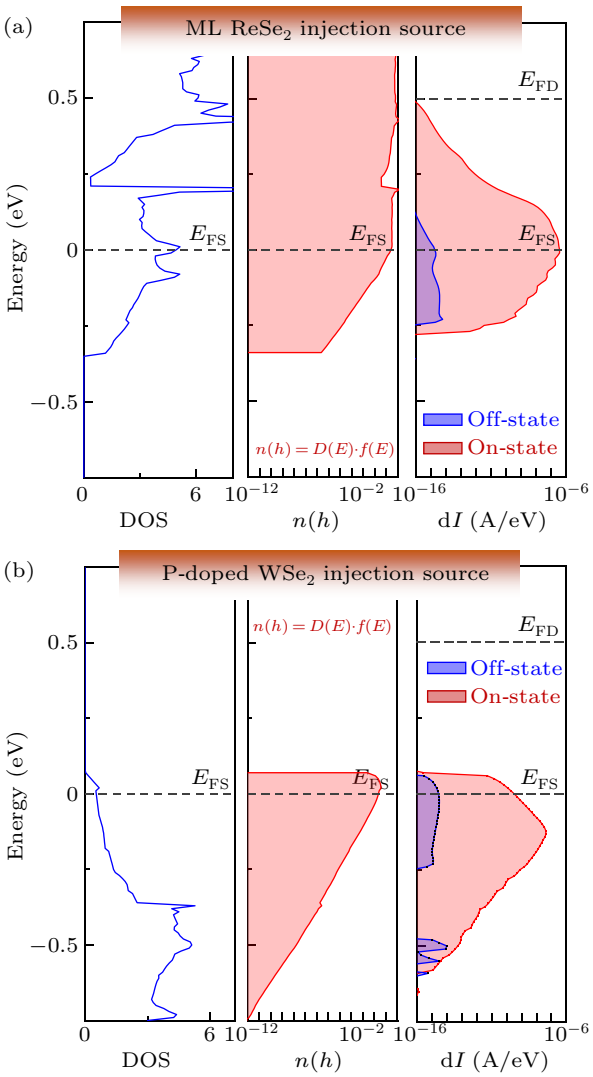


Fig. 3. Comparisons of injection mechanism between (a) $ReSe_2$ cold-source and (b) p-type doped WSe_2 source. The panels from left to right are respectively the DOS of the injection source, corresponding hole density $n(h)$, and the spectral current $\mathrm{d}I$ at the on/off state.

The DOSs and hole distributions $n(h)$ of the ReX_2 and TcX_2 monolayers are presented in Fig. 4(c). The exponentially decaying hole density in traditional metals is plotted in blue lines for comparison. For $TcSe_2$ ($ReSe_2$) monolayer, the hole tails with energy lower than 0.24 (0.35) eV are effectively cut off by the sub-gap below the Fermi level, exhibiting a typical cold metal characteristic like the role of $NbTe_2$ in CS-nFETs.[33] While for the TcS_2 (ReS_2) monolayer, the overall decaying DOSs with energy result in the superexponentially decreasing $n(h)$ and further the suppression of thermal tail contribution to the off-state, exhibiting a Dirac source char-

acteristic similar to n-doped graphene.[25] It is the suppression or cut-off of the hole tails that breaks the SS limitation in traditional MOSFETs and obtains the sub-thermal switches in CS-FETs.

To benchmark the studied device performance against the international technology roadmap for semiconductors (ITRS),[41] we set off-state currents around 5×10^{-5} μA/μm according to the low-power applications in ITRS requirements. We re-extracted the on-state currents and current on/off ratio. Moreover, we calculated the intrinsic delay time (τ), and power dissipation (PDP), which reflect the switching speed and energy consumption, respectively. τ is calculated by $\tau = (Q_{on} - Q_{off})/I_{on}$, and PDP is defined by PDP $= (Q_{on} - Q_{off}) \cdot V_{ds}/W$, in which $Q_{on/off}$ is the charges at on/off-state and W is channel width. The calculated results are all listed in Table 1. When employing ReX_2 and TcX_2 as sources, the WSe_2-CSFETs exhibit higher I_{on}/I_{off}, smaller τ, and lower PDP than the normal WSe_2-FET. Although the I_{on} of WSe_2-CSFETs cannot reach the ITRS requirements, the τ and PDP both can fulfill the ITRS standard, exhibiting fast speed and lower consumption. Besides, we further compare the WSe_2-CSFETs with some other 2D p-type FETs reported in the paper, including silicane,[42] Bi_2O_2Se,[43] InSe,[44] and $MoSi_2N_4$[45] monolayers. It is found that the studied WSe_2-CSFETs possess much higher I_{on}, smaller τ, and lower PDP than the silicane- and Bi_2O_2Se-based pFETs. Although the ions of WSe_2-CSFETs are smaller than the reported $MoSi_2N_4$- and InSe-based pFETs, the τ and PDP are lower than the $MoSi_2N_4$ FET and the PDP is comparable with the InSe FET. In conclusion, the ReX_2 and TcX_2 metals can effectively improve the WSe_2 FET performance and enhance the competitiveness of the emerging 2D FETs in future low-power transistor applications.

Table 1. Performance comparisons of the WSe_2 MOSFET and CS-FETs against ITRS requirements for the low-power transistors and with other 2D p-type FETs.

	L_g (nm)	V_{ds} (V)	I_{off} (μA/μm)	I_{on} (μA/μm)	I_{on}/I_{off}	SS (mV/dec)	τ (ps)	PDP (fJ/μm)
WSe_2-FET	6.6	0.5	5.4×10^{-5}	32	5.9×10^5	64	3.4	0.066
WSe_2-CSFET	6.6	0.5	$(2.5–6.5) \times 10^{-5}$	76–133	$(1.9–3.1) \times 10^6$	29–38	0.42–0.78	0.034–0.042
Silicane[42]	5	0.66	5.1×10^{-5}	3.12	6.1×10^4	97	19	0.039
Bi_2O_2Se[43]	5	0.64	5×10^{-5}	0.2	4×10^3	–	1200	0.16
InSe[44]	5	0.64	5×10^{-5}	490	9.8×10^6	64	0.11	0.034
$MoSi_2N_4$[45]	5	0.64	5×10^{-5}	213	4.3×10^6	71	0.916	0.125
ITRS[41]	5.9	0.64	5×10^{-5}	295	5.9×10^6	–	1.493	0.28

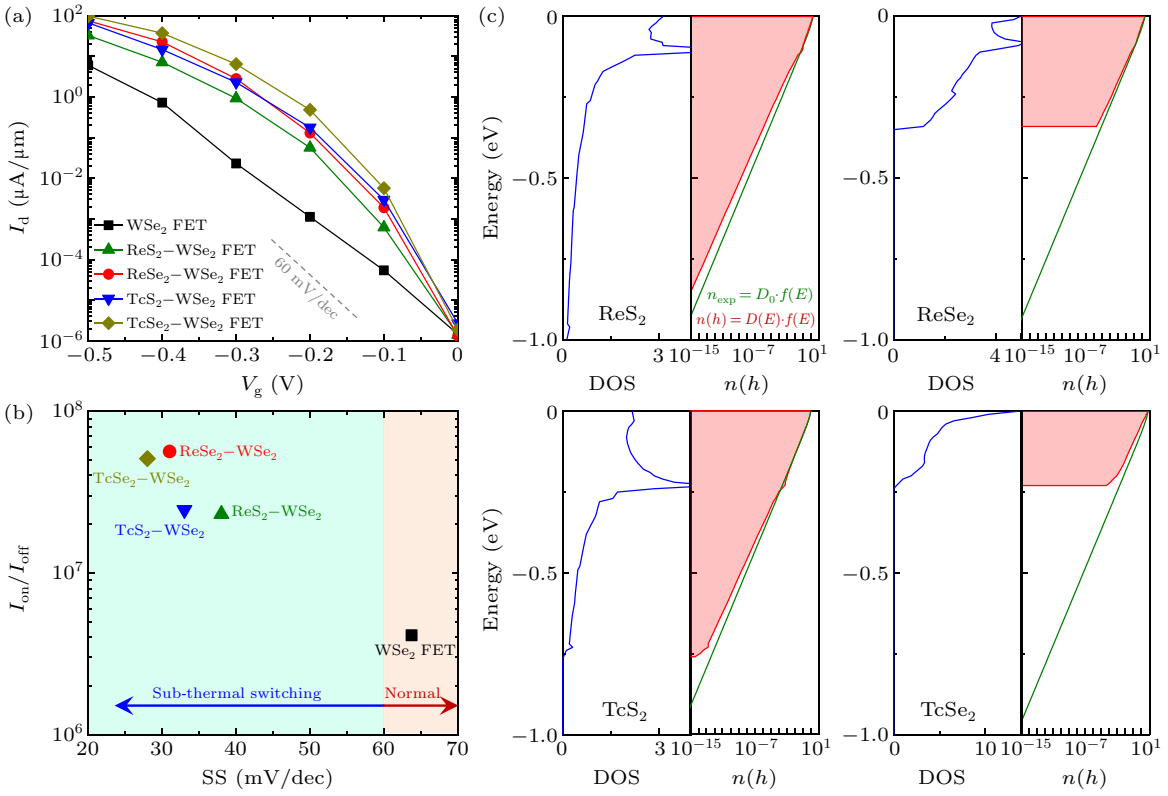


Fig. 4. Transfer characteristics of WSe_2 FETs with different cold metals and p-doped WSe_2 as the injection source. (b) Switching performance (I_{on}/I_{off} and SS) comparisons of WSe_2 FETs with different injection sources. (c) The cold metal DOS and corresponding hole density $n(h)$, E_F is set to 0 eV. The exponentially decaying hole distribution n_{exp} is shown in the blue line.

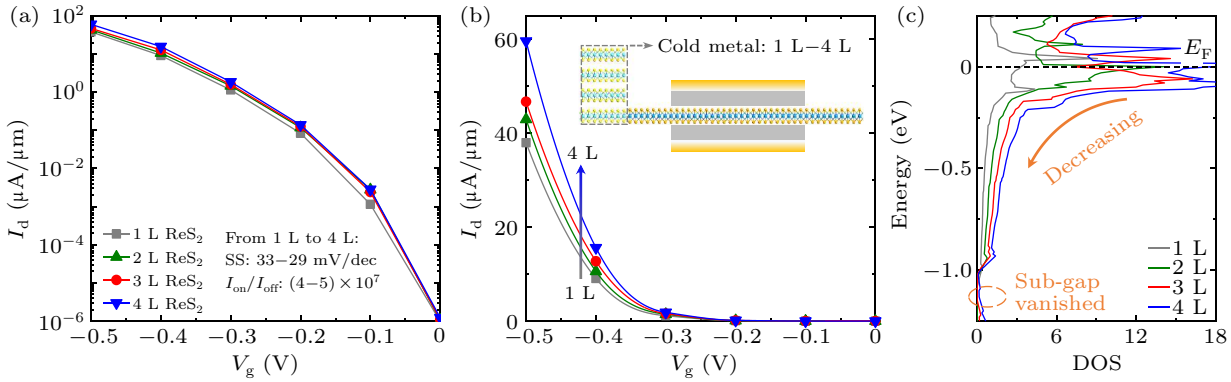


Fig. 5. (a) and (b) Transfer characteristics of WSe_2 FETs with different thicknesses ReS_2 layers (1L–4L) as injection sources: (a) logarithm and (b) linear coordinates. Inset is the FET schematic structure. (c) DOS of ReS_2 layers with different thicknesses (1L–4L).

We have revealed the cold source effects of the monolayer ReX_2 and TcX_2. However, accessing singlelayer TMDs remains challenging in practical 2D device fabrications. Taking ReS_2 as an example, we proceed to study the FET's performance based on multilayer 2D cold metals. The single-layered (1L), bi-layered (2L), tri-layered (3L), and quad-layered (4L) ReS_2 are respectively used as the injection source of WSe_2 pFETs (see the inset of Fig. 5(b)). The simulated switching performances are shown in Figs. 5(a)–5(b). It is found that for the 1L–4L ReS_2 injection sources, the WSe_2 pFETs show similar I_d–V_g curves, which all can break the thermal limitation and achieve the steep SS with values of 29–33 mV/dec. The corresponding I_{on}/I_{off} is as high as (4–5)×10^7. Besides, as shown in the linear coordinate (Fig. 5(b)), the I_{on} increases gradually from 38 μA/μm to 60 μA/μm with the increasing layers of the ReS_2 source. This relates to the carrier concentration in the source electrode. Figure 5(c) further presents the calculated DOS of the 1L–4L ReS_2 injection sources. The DOS decreasing tendency is preserved for various ReS_2 layers, which leads to the localization of hole distribution around the E_F and is conducive to obtaining the steep switches. Besides, we further analyze the DOS of the other three cold metals with different thicknesses (see Fig. S3 of the supporting information). The multilayer ReX_2 and TcX_2 all preserve their cold-metal characteristics, and are anticipated to break the SS limitations while serving as the injection source.

4. Conclusion

The TcX_2 and ReX_2 cold metals were proposed as the injection sources in p-type CS-FETs to achieve sub-thermal switches. First-principles calculations revealed the cold metal characteristics of TcX_2 and ReX_2 with a sub-gap below the Fermi level, which can effectively suppress or cut off the thermal tails of holes. Comprehensive transport simulations demonstrated that the steep SS (29–38 mV/dec) and high I_{on}/I_{off} ((2.3–5.6)×10^7) were achieved in WSe_2 CS-pFETs with TcX_2 and ReX_2 injection sources, significantly super to those of WSe_2 MOSFET (64 mV/dec and 4.1 × 10^6). Depending on their DOS features, the super-exponential decay of hole tails and direct cutting-off occurred for TcS_2 (ReS_2) and $TcSe_2$ ($ReSe_2$) injection sources, respectively. Moreover, by varying the thickness of cold metal from 1L to 4L, the steep switching properties could be obtained in ReS_2–WSe_2 FETs.

Acknowledgments

Project was supported by the National Natural Science Foundation of China (Grant Nos. 62034006, 92264201, and 62104134) and the Natural Science Foundation of Shandong Province of China (Grant Nos. ZR2023QF076 and ZR2023QF054).

References

[1] Waldrop M M 2016 *Nature* **530** 144
[2] Takagi S, Iisawa T, Tezuka T, Numata T, Nakaharai S, Hirashita N, Moriyama Y, Usuda K, Toyoda E, Dissanayake S, Shichijo M, Nakane R, Sugahara S, Takenaka M and Sugiyama N 2008 *IEEE Trans. Electron Devices* **55** 21
[3] Ionescu A M and Riel H 2011 *Nature* **479** 329
[4] Kim S, Myeong G, Shin W, Lim H, Kim B, Jin T, Chang S, Watanabe K, Taniguchi T and Cho S 2020 *Nat. Nanotechnol.* **15** 203
[5] Sarkar D, Xie X, Liu W, Cao W, Kang J, Gong Y, Kraemer S, Ajayan P M and Banerjee K 2015 *Nature* **526** 91
[6] Appenzeller J, Lin Y M, Knoch J and Avouris P 2004 *Phys. Rev. Lett.* **93** 196805
[7] Zhou W, Zhang S, Wang Y, Guo S, Qu H, Bai P, Li Z and Zeng H 2020 *Adv. Electron. Mater.* **6** 1901281
[8] Zhang S, Guo S, Chen Z, Wang Y, Gao H, Gomez-Herrero J, Ares P, Zamora F, Zhu Z and Zeng H 2018 *Chem. Soc. Rev.* **47** 982
[9] Ersan F, Kecik D, Ozcelik V, Kadioglu Y, Akturk O, Durgun E, Akturk E and Ciraci S 2019 *Appl. Phys. Rev.* **6** 021308
[10] Hong Y, Liu Z, Wang L, Zhou T, Ma W, Xu C, Feng S, Chen L, Chen M, Sun D, Chen X, Cheng H and Ren W 2020 *Science* **369** 670
[11] Wang L, Shi Y, Liu M, Zhang A, Hong Y, Li R, Gao Q, Chen M, Ren W, Cheng H, Li Y and Chen X 2021 *Nat. Commun.* **12** 2361
[12] Cao L, Zhou G, Wang Q, Ang L K and Ang Y 2021 *Phys. Rev. Appl.* **118** 013106
[13] Wang Q, Cao L, Liang S, Wu W, Wang G, Lee C, Ong W, Yang H, Ang L, Yang S and Ang Y 2021 *NPJ 2D Mater. Appl.* **5** 71
[14] Appenzeller J, Lin Y M, Knoch J and Avouris P 2004 *Phys. Rev. Lett.* **93** 196805
[15] Ionescu A M and Riel H 2011 *Nature* **479** 329
[16] Shin G H, Koo B, Park H, Woo Y, Lee J E and Choi S Y 2018 *ACS Appl. Mater. Interfaces* **10** 40212
[17] Sarkar D, Xie X, Liu W, Cao W, Kang J, Gong Y, Kraemer S, Ajayan P M and Banerjee K 2015 *Nature* **526** 91
[18] Cao W, Sarkar D, Khatami Y, Kang J and Banerjee K 2014 *AIP Adv.* **4** 067141

[19] Lv Y, Qin W, Huang Q, Chang S, Wang H and He J 2017 *IEEE Trans. Electron Devices* **64** 2694
[20] Brahma M, Kabiraj A, Saha D and Mahapatra S 2018 *Sci. Rep.* **8** 5993
[21] Jo J and Shin C 2016 *IEEE Electron Device Lett.* **37** 245
[22] Kwon D, Chatterjee K, Tan A J, Yadav A K, Zhou H, Sachid A B, Reis R D, Hu C and Salahuddin S 2018 *IEEE Electron Device Lett.* **39** 300
[23] Guo S, Prentki R J, Jin K, Chen C L and Guo H 2021 *IEEE Trans. Electron Devices* **68** 911
[24] Yu Z, Wang H, Li W, Xu S, Song X, Wang S, Wang P, Zhou P, Shi Y, Chai Y and Wang X 2017 *Proceedings of IEEE International Electron Device Meeting (IEDM)*, December 2–6, 2017, San Francisco, USA, pp. 23.6.1
[25] Qiu C, Liu F, Xu L, Deng B, Xiao M, Si J, Lin L, Zhang Z, Wang J, Guo H, Peng H and Peng L M 2018 *Science* **361** 387
[26] Liu F, Qiu C, Zhang Z, Peng L M, Wang J, Wu Z and Guo H 2018 *Proceedings of IEEE International Electron Device Meeting (IEDM)*, December 1–5, 2018, San Francisco, USA, pp. 31.2.1
[27] Tang Z, Liu C, Huang X, Zeng S, Liu L, Li J, Jiang Y G, Zhang D W and Zhou P 2021 *Nano Lett.* **21** 1758
[28] Liu F, Qiu C, Zhang Z, Peng L M, Wang J and Guo H 2018 *IEEE Trans. Electron Devices* **65** 2736
[29] Wang Q, Sang P, Ma X, Wang F, Wei W, Zhang W, Li Y and Chen J 2018 *Proceedings of IEEE International Electron Device Meeting (IEDM)*, December 12–18, 2018, San Francisco, USA, pp. 22.4.1
[30] Wang Q, Sang P, Wang F, Wei W, Li Y and Chen J 2021 *Appl. Phys. Express* **14** 074003
[31] Nandan K, Bhowmick B, Chauhan Y and Agarwal A 2023 *Phys. Rev. Appl.* **19** 064058
[32] Wang Q, Sang P, Wang F, Wei W and Chen J 2021 *IEEE Trans. Electron Devices* **68** 4758
[33] Liu F 2020 *Phys. Rev. Appl.* **13** 064037
[34] Shin W, Myeong G, Sung K, Kim S, Lim H, Kim B, Jin T, Park J, Watanabe K, Taniguchi T, Liu F and Cho S 2022 *Appl. Phys. Lett.* **120** 243506
[35] Smidstrup S, Markussen T, Vancraeyveld P, *et al.* 2020 *J. Phys. Condens. Matter* **32** 015901
[36] Van Setten M J, Giantomassi M, Bousquet E, Verstraete M J, Hamann D R, Gonze X and Rignanese J M 2018 *Comput. Phys. Commun.* **226** 39
[37] Perdew J P, Burke K and Ernzerhof M 1996 *Phys. Rev. Lett.* **77** 3865
[38] Büttiker M, Imry Y, Landauer R and Pinhas S 1985 *Phys. Rev. B: Condens. Matter* **31** 6207
[39] Zhang Y, Yin L, Chu J, Shifa T, Xia J, Wang F, Wen Y, Zhan X, Wang Z and He J 2018 *Adv. Mater.* **30** 1803665
[40] Bertolazzi S, Brivio J and Kis A 2011 *ACS Nano* **5** 9703
[41] International technology roadmap for semiconductors (ITRS)
[42] Pan Y, Dai J, Xu L, Yang J, Zhang X, Yan J, Shi B, Liu S, Hu H, Wu M and Lu J 2020 *Phys. Rev. Appl.* **14** 024016
[43] Quhe R, Liu J, Wu J, Yang J, Wang Y, Li Q, Li T, Guo Y, Yang J, Peng H, Lei M and Lu J 2019 *Nanoscale* **11** 532
[44] Wang Y, Fei R, Quhe R, Li J, Zhang H, Zhang X, Shi B, Xiao L, Song Z, Yang J, Shi J, Pan F and Lu J 2019 *ACS Appl. Mater. Interfaces* **10** 23344
[45] Sun X, Song Z, Huo N, Liu S, Yang C, Yang J, Wang W and Lu J 2021 *J. Mater. Chem. C* **9** 14683